BENTHAM SCIENCE

CrossMark

Current Medical Imaging

Content list available at: https://benthamscience.com/journals/cmir

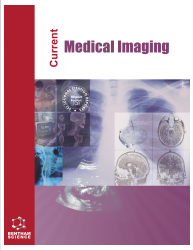

RESEARCH ARTICLE

Value of the Stretched Exponential and Fractional-order Model in Differentiating Hepatocellular from Intrahepatic Cholangiocarcinoma

Jinhuan Xie[1], Chenhui Li[1], Qianjuan Chen[1], Yidi Chen[2], Huiting Zhang[3] and Liling Long[1,4,5,*]

[1]*Department of Radiology, The First Affiliated Hospital of Guangxi Medical University, Nanning 5320021, China*
[2]*Department of Radiology, West China Hospital, Sichuan University, Chengdu 610044, China*
[3]*MR Scientific Marketing, Siemens Healthineers, Wuhan 430015, China*
[4]*Key Laboratory of Early Prevention and Treatment for Regional High Frequency Tumor (Guangxi Medical University), Ministry of Education, Nanning 532001, China*
[5]*Guangxi Key Laboratory of Immunology and Metabolism for Liver Diseases, Nanning 532001, China*

Abstract:

Background:

It remains unknown whether the parameters obtained using the Stretched Exponential Model (SEM) and Fractional Order Calculus (FROC) models can help distinguish Hepatocellular Carcinoma (HCC) from Intrahepatic Cholangiocarcinoma (ICC).

Objective:

This study aimed to evaluate the application value of the parameters of the 3.0T Magnetic Resonance Imaging (MRI) high-order SEM and FROC diffusion model in differentiating HCC and ICC.

Methods:

Patients with pathologically confirmed HCC and ICC were prospectively enrolled. Diffusion-weighted imaging scans with multiple b-values were acquired 2 weeks before the surgery. The original MRI images were fitted using the mono-exponential model, SEM, and FROC, and several parameters were obtained for the analysis.

Results:

In total, 74 patients with HCC and 21 with ICC were included in the study. Significant differences between the HCC and ICC groups were noted in the Apparent Diffusion Coefficient (ADC: $p = 0.007$), Distributed Diffusion Coefficient (DDC: $p < 0.001$), and Diffusion coefficient (D: $p < 0.001$), as each value was significantly lower in the HCC than in the ICC group. The area under the receiver operating characteristic curve of ADC, DDC, and D was 0.694, 0.812, and 0.825, respectively, and the most effective corresponding cut-off values were 1.135 $\mu m^2/ms$, 1.477 $\mu m^2/ms$, and 1.104 $\mu m^2/ms$, respectively.

Conclusion:

The diffusion parameters DDC from the SEM and D from the FROC model have been found to be more effective in discriminating HCC and ICC than the ADC from the mono-exponential model. Combining these quantitative parameters can improve the MRI's diagnostic accuracy, providing useful information for the preoperative differential diagnosis between HCC and ICC.

Keywords: Hepatocellular carcinoma, Intrahepatic cholangiocarcinoma, Stretched exponential model, Fractional-order calculus model, Differential diagnosis, Prospective study.

Article History	Received: May 23, 2024	Revised: October 03, 2024	Accepted: October 11, 2024

1. INTRODUCTION

Primary liver cancers include the two most common pathological types: Hepatocellular Carcinoma (HCC) and Intrahepatic Cholangio Carcinoma (ICC). These forms present marked differences in terms of pathogenesis, biological

behavior, histopathological morphology, treatment, and prognosis. HCC accounts for approximately 75 85% of primary liver cancers and ICC for 10–15%, respectively [1].

The stage of HCC development determines the clinical treatment plan [2]. Most patients with early and mid-stage HCC are eligible for non-drug treatments, such as hepatectomy, transcatheter chemoembolization, and liver transplantation [3, 4]. Radiofrequency ablation is a key treatment option for patients with small liver tumors or those who cannot undergo resection [5]. For patients with advanced-stage HCC, systemic treatment is prioritized, with a combination of transarterial chemoembolization and systemic therapies shown to produce antitumor efficacy and synergy [6]. Molecular-targeted therapies, immunotherapy, and monoclonal antibody drugs are considered first line treatments. Multi-protocol and personalized approaches have improved progression-free survival and overall survival in patients with HCC [7 - 9].

ICC originates from the epithelial cells of the intrahepatic bile duct; it is typically located in the distal tract of the bile duct within the liver, and it grows infiltratively along its mucosa. It presents no obvious symptoms and signs in the early stages; thus, most patients are diagnosed only at an advanced stage of the disease. Currently, the only curative treatments available are surgical resection or liver transplantation [8]; however, adjuvant chemotherapy and targeted therapy can improve the quality of life and prolong progression free survival of patients with unresectable tumors or intrahepatic or distant metastasis [10, 11].

An accurate preoperative differential diagnosis between these histological types is crucial owing to the vast differences in surgical methods, treatment strategies, and prognosis between HCC and ICC. HCC is the only tumor that can be diagnosed using imaging; however, atypical HCC and ICC have similar imaging features, and it is often difficult to distinguish between them using conventional imaging methods [12]. Diffusion Weighted Imaging (DWI) is a non-invasive functional Magnetic Resonance Imaging (MRI) technique. Several pathological features, such as tumor infiltration, trauma, inflammation, and ischemia, can alter the tissue histological structure and affect the water diffusion characteristics, resulting in specific DWI signal patterns [13]. The Apparent Diffusion Coefficient (ADC) is calculated from DWI images to quantify the diffusion of water molecules within tissues and assess different biological characteristics [14 - 16]. The water diffusion displacement in highly heterogeneous tumor tissues deviates significantly from the Gaussian distribution; therefore, the ADC based on the traditional mono-exponential DWI model cannot fully reflect the diffusion properties of water in tumor tissues, and its application has obvious limitations [17, 18]. In contrast, the Stretched Exponential Model (SEM), described by Bennett *et al*., and the Fractional Order Calculus (FROC) model, first proposed by Zhou *et al*., have attracted increasing attention to overcome these issues [19, 20].

The SEM quantifies voxel heterogeneity using the Distributed Diffusion Coefficient (DDC) and intravoxel water molecular diffusion heterogeneity (α) to describe the complexity and diversity of tumor tissues and their microstructures. The SEM can reflect the physiological characteristics of biological tissues, the heterogeneity of the diffusion rate between voxels, and the different distribution and diffusion effects of water molecules in each voxel [21]. In previous studies, the SEM has been used to characterize hepatic fibrosis, microvascular invasion of liver cancer, and esophageal cancer grade, and to evaluate the efficacy of breast cancer treatments [22 - 26].

The FROC model is a new method to evaluate the non-Gaussian distribution of water molecules. It uses the diffusion coefficient (D), fractional-order derivative in space (β), and spatial parameter (μ) to describe the complex diffusion processes in highly heterogeneous tissues, such as tumors [27]. Previous studies have reported the FROC model to be useful in determining the pathological characteristics of different diseases, tumor grading, and the differential diagnosis between benign and malignant tumors [28 - 33]. However, it remains to be determined whether the parameters obtained using the SEM and FROC models can be helpful in distinguishing HCC and ICC on the basis of multiple b-value (0-3000 s/mm^2) DWI scanning sequences.

The purpose of this study was to evaluate the feasibility of the SEM and FROC models in the non-invasive differential diagnosis of HCC and ICC by prospectively collecting DWI images of these tumors with multiple b-values (0-3000 s/mm^2) and dividing them according to postoperative pathological data. We aimed to provide a reference for early clinical diagnosis and treatment to improve the prognosis of patients with HCC and ICC. This follow-up clinical study has been based on the article titled "Potential Value of the Stretched Exponential and Fractional Order Calculus Model in Discriminating Between Hepatocellular Carcinoma and Intrahepatic Cholangio-carcinoma: An Animal Experiment of Orthotopic Xenograft Nude Mice," published in *Current Medical Imaging* [34].

2. MATERIALS AND METHODS

2.1. Participants

Participants were prospectively recruited from our institution from June 2021 to November 2022. Patients with suspected malignant lesions, identified on abdominal ultrasonography or computed tomography examinations, underwent MRI scanning with conventional preoperative sequences and multiple DWI sequences with several b-values (0-3000 s/mm^2). Afterward, they underwent liver cancer resection within 2 weeks.

The inclusion criteria were as follows: (1) MRI examination and no treatment related to liver cancer before surgery; (2) radical resection surgery; and (3) postoperative pathological examination confirming HCC or ICC.

* Address correspondence to this author at the Department of Radiology, The First Affiliated Hospital of Guangxi Medical University, Nanning 530021, China, Key Laboratory of Early Prevention and Treatment for Regional High Frequency Tumor (Guangxi Medical University), Ministry of Education, Nanning 532001, China and Key Laboratory of Early Prevention and Treatment for Regional High Frequency Tumor (Guangxi Medical University), Ministry of Education, Nanning 532001, China; Tel: +86 13807712604;
E-mail: cjr.longliling@vip.163.com

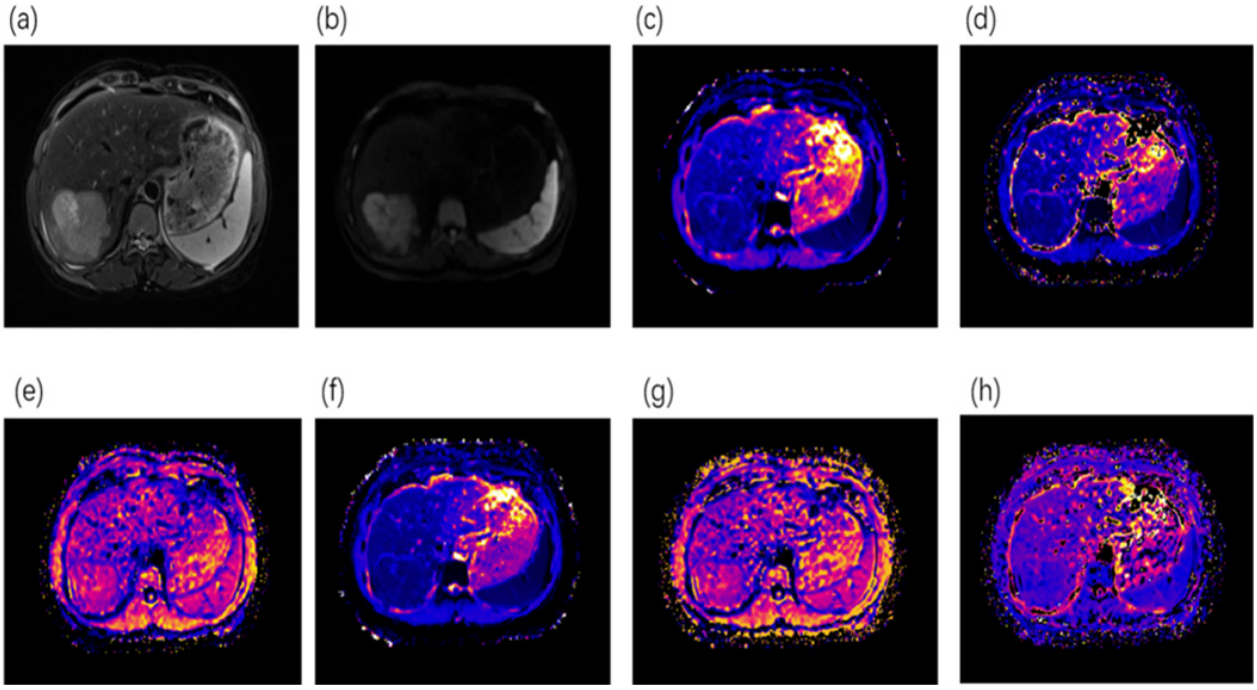

Fig. (1). MRI images of a patient with pathologically confirmed hepatocellular carcinoma.
(**a**) Cross-sectional T2-weighted fat-suppression image; (**b**) Diffusion Weighted Image (DWI) at b = 1000 s/mm^2; (**c**) Apparent Diffusion Coefficient (ADC) map; (**d**, **e**) parameter maps of the Stretched Exponential Model (SEM): Distributed Diffusion Coefficient (DDC) and diffusion heterogeneity coefficient (α), respectively; (**f**, **g**, **h**) parameter maps of the Fractional Order Calculus (FROC) model: diffusion coefficient (D), spatial fractional parameter (β), and spatial parameter (μ), respectively. MRI: magnetic resonance imaging.

The following exclusion criteria were considered: (1) distant metastases; (2) lesion diameter as seen on MRI images < 1 cm; (3) low MRI image quality; (4) previous history of other malignant tumors; and (5) no immunohistochemical results after surgery.

The study was approved by the medical ethics committee of the First Affiliated Hospital of Guangxi Medical University (approval no. 2022-KY-E-271), and all patients provided written informed consent. SAGER guidelines were followed.

2.2. MRI Scans

All images were acquired using a 3.0T MRI scanner (MAGNETOM Prisma, Siemens, Munich, Germany), using a 16-channel body coil combined with respiratory gating.

A DWI sequence of free breath plus breath navigation was acquired, and three orthogonal diffusion-coding directions were set. The 10 b-values used were 0, 20, 50, 100, 150, 200, 600 [1], 1000 [2], 2000 [4], and 3000 [6] s/mm^2. The detailed parameters of the DWI sequence are as follows: Repetition Time (TR) = 4900 ms, Echo Time (TE) = 57 ms, Field of View (FOV) = 380 mm × 261 mm, FOV phase = 68.8%, matrix = 88 × 128, layer thickness = 5.0 mm, layer spacing = 6.4 mm, bandwidth = 2442 Hz/pixels, and parallel acquisition acceleration factor = 2, which shortened the scanning time and reduced image distortion.

The other scan sequences and specific parameters are as follows: conventional T1-weighted Images (T1WI): TR = 6.51 ms, TE = 2.61 ms, inversion angle = 12°, slice thickness = 5.0 mm, layer spacing = 2.0 mm, voxel size = 0.4 × 0.4 × 5.0 mm; cross-sectional T2WI fat-suppression sequence: TR = 2700 ms, TE = 54 ms, inversion angle = 110°, slice thickness = 5.0 mm, layer spacing = 2.0 × 0.2 × 5.0 mm; coronal T2WI sequence: TR = 3000 ms, TE = 82 ms, inversion angle = 180°, slice thickness = 5.0 mm, interval = 2.0 mm, FOV read = 420 mm, FOV phase = 100%, voxel size = 0.2 × 0.2 × 1.2 mm.

2.3. Image Post-processing and Quantitative Measurements

After the scan was completed, the DWI DICOM images were imported into the post-processing software Body-DiffusionLab (BoDiLab, ChengDu ZhongYing Medical Technology Co., Ltd., ChengDu, China) and used to calculate the ADC values and the various parameters for the SEM and FROC models (Figs. **1** and **2**).

The mono-exponential model to fit the DWI data was estimated as follows:

$$\frac{Sb}{S0} = \exp(-b \times ADC),$$

Where, S0 and Sb are the signal intensities for b-values of 0 and 1000 s/mm^2, respectively, and ADC is the apparent diffusion coefficient.

The SEM to fit the DWI data was calculated with the following formula:

$$\frac{Sb}{S0} = \exp[-(b \times DDC)]\,\alpha,$$

Where, S0 and Sb are the same as above; DDC is the distributed diffusion coefficient (in $\mu m^2/ms$), and α represents the intravoxel water diffusion heterogeneity (unitless; $0 < \alpha \leq 1$). The Levenberg-Marquardt non-linear fitting algorithm was adopted to fit the diffusion images obtained at 10 different b-values to the SEM voxel by voxel.

Finally, the FROC model was estimated as follows:

$$\frac{Sb}{S0} = \exp[-D\mu 2(\beta - 1)(\gamma Gd\delta)2\beta(\Delta - (2\beta - 1)(2\beta + 1)\delta)],$$

Where, S0 and Sb are described as above; Gd, δ, and Δ are the amplitude, pulse width, and lobe separation of the diffusion gradient, respectively; D is the diffusion coefficient (unit: $\mu m^2/ms$); β is the fractional-order derivative in space (unitless; $0 < \beta \leq 1$); and μ is a spatial parameter (μm). The Levenberg-Marquardt non-linear fitting algorithm was again used to fit the diffusion images to the FROC model.

All the post processed ADC, SEM, and FROC parameter images were quantified using Body-DiffusionLab and analyzed by two radiologists with more than 5 years of experience in liver MRI diagnosis, blinded to the histopathological results. The Volume of Interest (VOI) was manually segmented on DWI images with b = 1000, using T2WIs as a reference, and included all the tumor layers visible on each parameter image; however, the tumor areas showing bleeding or necrosis were carefully omitted in the VOIs for more accurate results. Subsequently, the VOIs were automatically superimposed on all other parameter images at the same level to calculate the parameter values. The final value for each parameter was obtained, averaging the values calculated by the two radiologists.

2.4. Statistical Analysis

SPSS 26.0 (IBM, Armonk, NY, USA) was used to analyze the data. The Intra-class Correlation Coefficient (ICC) was used to evaluate the consistency of ADC, SEM, and FROC model parameters calculated by the two radiologists (< 0.50: poor agreement; 0.50–0.75: moderate; 0.75–0.90: good; > 0.90: very good agreement). The quantitative data have been expressed as mean ± standard deviation, and the Shapiro–Wilk or Kolmogorov–Smirnov test was used to assess the normality of their distribution. The differences in diffusion parameters between the HCC and ICC groups were examined with an independent sample t-test (normal distribution) or Mann-Whitney U test (non-normal distribution). A Receiver Operating Characteristic (ROC) curve was obtained for parameters with significant differences between the two groups, and the Area Under the Curve (AUC) was calculated to evaluate the diagnostic efficiency of each diffusion parameter. The optimal diagnostic threshold was selected on the basis of the maximum Youden index value, and the corresponding sensitivity and specificity values were calculated for each variable. Statistical significance was set at $p < 0.05$.

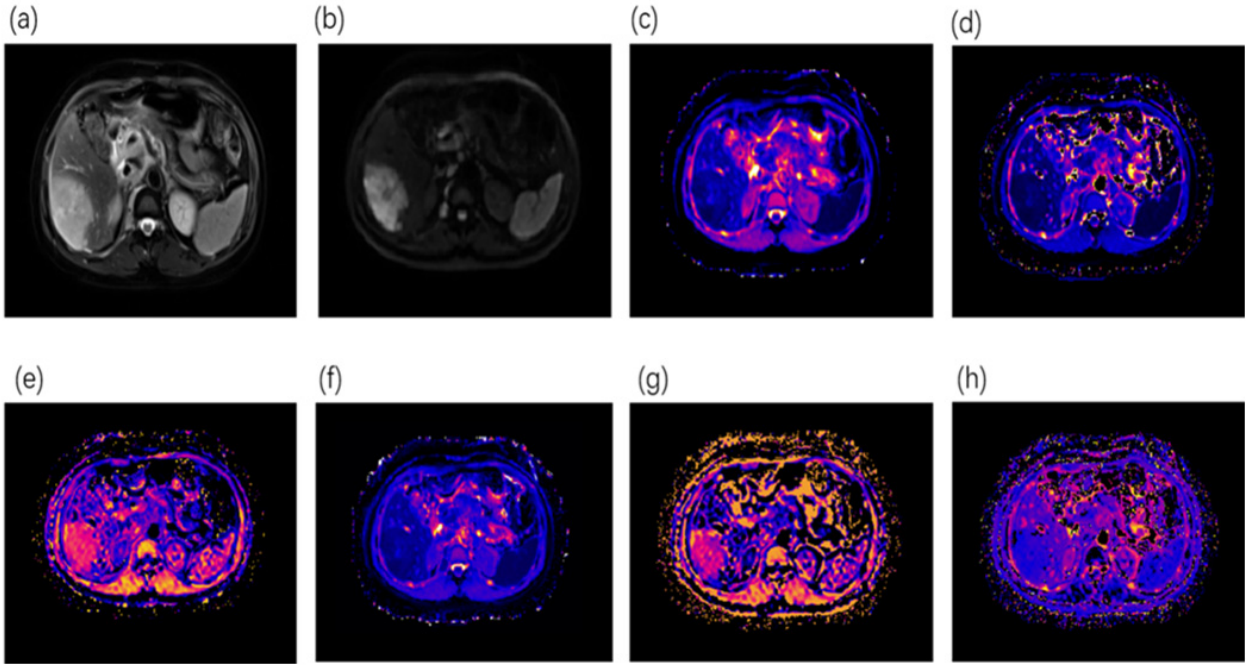

Fig. (2). MRI images of a patient with pathologically confirmed intrahepatic cholangiocarcinoma.
(**a**) Cross-sectional T2-weighted fat-suppression image; (**b**) Diffusion Weighted Image (DWI) at b = 1000 s/mm^2; (**c**) Apparent Diffusion Coefficient (ADC) map; (**d**, **e**) parameter maps of the Stretched Exponential Model (SEM): Distributed Diffusion Coefficient (DDC) and diffusion heterogeneity coefficient (α), respectively; (**f**, **g**, **h**) parameter maps of the Fractional Order Calculus (FROC) model: diffusion coefficient (D), spatial fractional parameter (β), and spatial parameter (μ), respectively. MRI: magnetic resonance imaging.

3. RESULTS

In total, 95 patients with primary liver cancer were recruited for the study, including 74 with HCC and 21 with ICC. The mean age in the HCC group was 52.5 ± 9.5 years, and 80% of patients were male; the mean maximum tumor diameter was 6.35 ± 3.56 cm. In the ICC group, the mean age was 58.9 ± 8.8 years, and 57% of patients were male; the mean maximum tumor diameter was 5.71 ± 3.25 cm. The main clinical and pathological data of the patients are shown in Table **1**.

3.1. Comparisons of SEM and FROC Parameters between the HCC and ICC Groups

The analysis of the consistency between the two radiologists gave the following ICC results: ADC = 0.833, DDC = 0.851, α = 0.822, D = 0.838, β = 0.884, and μ = 0.897, showing a good agreement (Table **2**). In the between-group comparison of all quantitative diffusion parameters, significant differences emerged in the ADC ($p = 0.007$), DDC of the SEM ($p < 0.001$), and D of the FROC model ($p < 0.001$); all these values were significantly lower in the HCC than in the ICC group (Fig. **3**). In contrast, no statistically significant differences between the groups were noted in the α, β, and μ values ($p = 0.893$, $p = 0.560$, $p = 0.979$, respectively). Detailed data are shown in Table **3**.

3.2. Diagnostic Performance of the Diffusion Metrics

The ADC, DDC, and D were analyzed with the ROC curve; the overall diagnostic efficacy of D and DDC was higher, with AUC of 0.825 and 0.812, respectively, whereas for the ADC, the AUC was 0.694 (Fig. **4**). However, D and DDC exhibited high specificity (98.65% and 85.14%, respectively) and low sensitivity (57.14% and 66.67%); in contrast, the ADC showed higher sensitivity (85.71%) and lower specificity (60.81%). These results are summarized in Table **4**.

The diffusion coefficient (D) exhibited the best diagnostic performance [Area Under the Curve (AUC): 0.825, 95% Confidence Interval (CI): 0.722–0.887, sensitivity: 57.14%, specificity: 98.65%), followed by the Distributed Diffusion Coefficient (DDC) (AUC: 0.812, 95% CI: 0.719–0.885, sensitivity: 66.67%, specificity: 85.14%), whereas the Apparent Diffusion Coefficient (ADC) demonstrated a lower diagnostic efficacy (AUC: 0.694, 95% CI: 0.591–0.784, sensitivity: 85.71%, specificity: 60.81%).

Table 1. Clinical and pathological data of the patients.

-	HCC Group (n = 74)	ICC Group (n = 21)	P
Maximum diameter (cm)	6.35 ± 3.56 (2.2-18.0)	5.71 ± 3.25 (1.8-15.0)	0.067
Age (years)	52.5 ± 9.5 (24-77)	58.9 ± 8.8 (41-71)	0.387
Sex	-	-	0.617
Male	59	12	-
Female	15	9	-
Etiology	-	-	0.524
Hepatitis B virus	69	18	-
Other	5	3	-
Microvascular invasion	-	-	0.071
Yes	32	6	-
No	42	15	-

Note: The data are expressed as mean ± standard deviation (range) or number, as appropriate. HCC: hepatocellular carcinoma; ICC: intrahepatic cholangiocarcinoma.

Table 2. Parameter values in the hepatocellular carcinoma and intrahepatic cholangiocarcinoma groups and consistency analysis between the two radiologists.

Parameters[a]	Radiologist 1		Radiologist 2		ICC	95% CI
	HCC Group	ICC Group	HCC Group	ICC Group		
ADC	1.223 ± 0.324	1.311 ± 0.288	1.235 ± 0.282	1.424 ± 0.318	0.833	0.834–0.926
DDC	1.238 ± 0.560	1.614 ± 0.457	1.306 ± 0.575	1.603 ± 0.346	0.851	0.815–0.934
α	0.567 ± 0.124	0.603 ± 0.112	0.619 ± 0.121	0.570 ± 0.130	0.822	0.882–0.918
D	0.812 ± 0.180	1.171 ± 0.373	0.868 ± 0.142	1.167 ± 0.388	0.838	0.863–0.913
β	0.680 ± 0.108	0.696 ± 0.089	0.668 ± 0.109	0.679 ± 0.091	0.884	0.833–0.902
μ	3.515 ± 0.485	3.462 ± 0.317	3.255 ± 0.351	3.375 ± 0.489	0.897	0.839–0.936

Note: [a]ADC, DDC, and D were measured in $\mu m^2/ms$, α and β in percentages, and μ in μm.
Abbreviations: HCC: hepatocellular carcinoma; ICC: intrahepatic cholangiocarcinoma; ICC: intraclass correlation coefficient; CI: confidence interval; ADC: apparent diffusion coefficient; DDC: distributed diffusion coefficient; α: diffusion heterogeneity coefficient; D: diffusion coefficient; β: spatial fractional parameter; μ: spatial parameter.

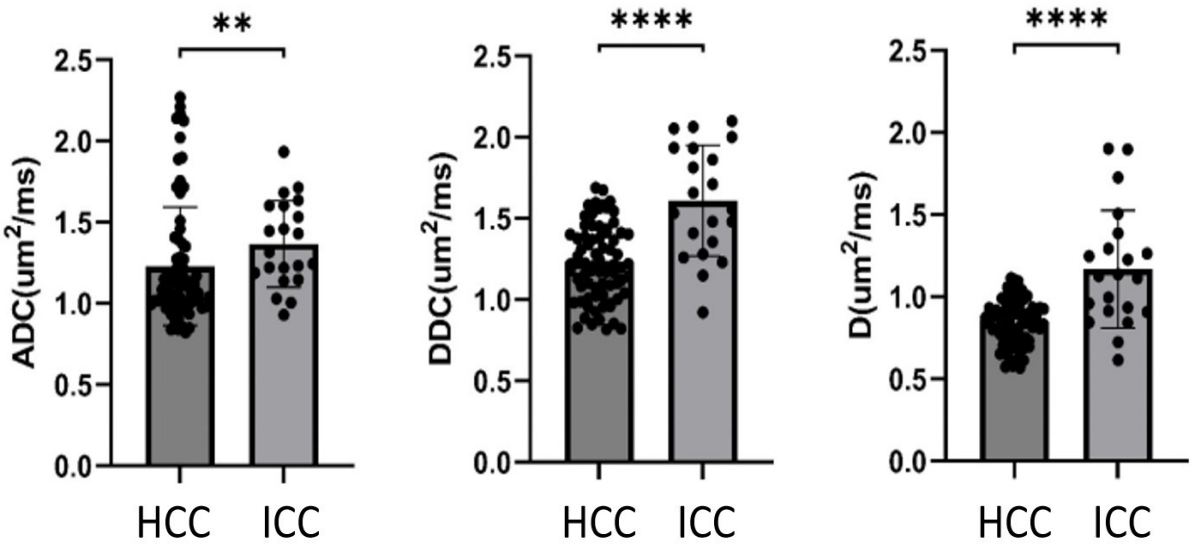

Fig. (3). Between-group comparisons of the parameters considered.
(**a**) The Apparent Diffusion Coefficient (ADC), (**b**) Distributed Diffusion Coefficient (DDC), and (**c**) diffusion coefficient (D) values in the Hepatocellular Carcinoma (HCC) group were significantly lower than those in the Intrahepatic Cholangiocarcinoma (ICC) group (**: $p < 0.01$; ****: $p < 0.001$).

Table 3. Comparison of the quantitative parameters of various diffusion models between the hepatocellular carcinoma and intrahepatic cholangiocarcinoma groups.

Parameters[a]	HCC Group	ICC Group	P
ADC	1.229 ± 0.366	1.367 ± 0.266	0.007*
DDC	1.272 ± 0.230	1.608 ± 0.341	< 0.001*
α	0.593 ± 0.104	0.587 ± 0.112	0.893
D	0.841 ± 0.135	1.169 ± 0.358	< 0.001*
β	0.674 ± 0.083	0.688 ± 0.083	0.560
μ	3.385 ± 0.425	3.419 ± 0.337	0.979

Note: [a] ADC, DDC, and D were measured in $\mu m^2/ms$, α and β in percentages, and μ in μm.
* indicates statistically significant differences.
Abbreviations: HCC: hepatocellular carcinoma; ICC: intrahepatic cholangiocarcinoma; ADC: apparent diffusion coefficient; DDC: distributed diffusion coefficient; α: diffusion heterogeneity coefficient; D: diffusion coefficient; β: spatial fractional parameter; μ: spatial parameter.

Table 4. Diagnostic efficacy of ADC, DDC, and D in discriminating hepatocellular carcinoma and intrahepatic cholangiocarcinoma.

Parameters	AUC	P	Sensitivity (%)	Specificity (%)	95% CI	Cut-off Value
ADC	0.694	0.001	85.71	60.81	0.591–0.784	1.135
DDC	0.812	< 0.001	66.67	85.14	0.719–0.885	1.477
D	0.825	< 0.001	57.14	98.65	0.722–0.887	1.104

Abbreviations: AUC: area under the curve; CI: confidence interval; ADC: apparent diffusion coefficient; DDC: distributed diffusion coefficient; D: diffusion coefficient.

4. DISCUSSION

Most primary liver cancers lack specific clinical features in the early stages. HCC and ICC are often diagnosed at the middle or late stages, with a poor prognosis. A research study by Xu *et al*. and Peng *et al*. has shown that genetic analysis has a strong predictive ability for the prognosis of primary liver cancer. A comprehensive assessment of a patient's genetic profile can help guide the selection of more effective treatment strategies. Therefore, it is crucial to use imaging techniques to accurately differentiate between HCC and ICC before treatment [35, 36]. DWI can differentiate several pathological changes in tissues, such as trauma, inflammation, ischemia, and necrosis, through measuring the ADC obtained with the mono-exponential DWI model; therefore, this type of sequence is widely used in clinical diagnosis [37 - 39]. The ADC is based on the assumption that the diffusion of water molecules in human tissues follows a free and random Gaussian distribution;

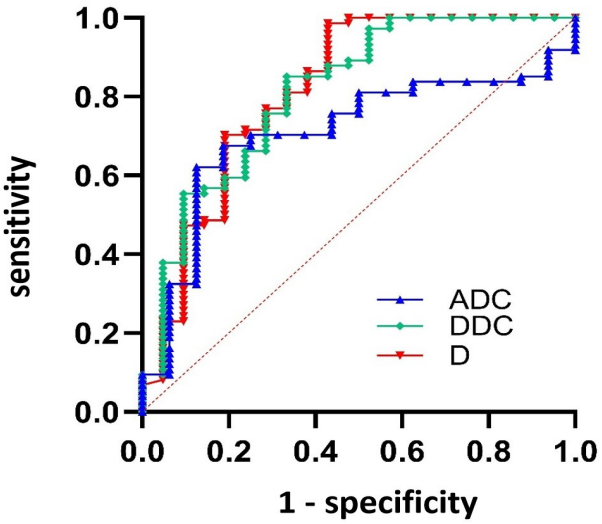

Fig. (4). Receiver operating characteristic curves of the parameters considered.

however, previous studies have shown that in the microstructure of tumor tissues, this motion deviates from the Gaussian distribution, affecting the accuracy of the ADC measurement [40]. We found the difference in ADC between the HCC and ICC groups to be statistically significant. However, the overall diagnostic efficacy of this parameter in differentiating these types of tumors was moderate. The ADC cannot accurately reflect the characteristics of water diffusion in highly heterogeneous tumor tissues; therefore, its clinical application in the differential diagnosis of malignant liver tumors is limited [13].

The SEM derives from the mono-exponential DWI model, and it can distinguish the tumor from the surrounding healthy tissues by measuring the signal attenuation caused by circuitous blood vessels and highly heterogeneous cell morphology, providing high accuracy in quantifying the heterogeneity in voxels [41]. Moreover, the DDC values derived from the SEM model represent the continuous distribution of diffusion coefficients from different tissue voxels and describe the average diffusion rate within them. We found a statistically significant difference in the mean DDC values between the groups; in the HCC group, this parameter was significantly lower than that in the ICC group, providing a higher diagnostic efficiency than that of the ADC. This difference may be explained by histopathology, as the DDC is mainly derived from hepatocytes. The HCC tumor cells are tightly arranged and grow in dense nests within the liver tissue; the tumor neovascularization increases and reduces the extracellular space, limiting the free movement of water molecules, and consequently, the DDC decreases. In contrast, ICC originates from the intrahepatic bile ducts; the tumor cells mostly surround the initial lesion, growing in a tubular, acinar, or cord shape, and allowing more freedom to the water diffusion movement compared to the HCC cells [42 - 44]. Another parameter derived from the SEM model, α, represents the heterogeneity of the water diffusion rate in voxels and describes the deviation between the signal attenuation and the one expected from the mono-exponential form. Therefore, it reflects the complexity of the tissue, and it ranges from 0 to 1 [45]. As reported by Bai *et al*., the α value in high-grade gliomas is significantly lower than that in low-grade gliomas, indicating that this parameter is affected by the water diffusion heterogeneity in tumor tissues [46]. However, we found no significant difference in α between HCC and ICC; this finding may be due to micronecrotic areas in the VOIs that cannot be identified by the naked eye on MRI images. In a previous study, α was reported to be heavily affected by tissue necrosis [21]. Additionally, the living cell density in the micronecrotic area was lower than that in the tumor tissue; thus, the tumor microstructure was more uniform [47], reducing the α accuracy. Moreover, both HCC and ICC are characterized by high tissue heterogeneity, and α may be insufficient to distinguish the different degrees of tissue heterogeneity.

The FROC model could also reveal the non-Gaussian distribution of water diffusion. Three parameters could be derived from it: D, β, and μ, describing the heterogeneity of the tumor tissue microstructure and representing the complex diffusion process; these parameters could complement the mono-exponential DWI model [48, 49]. D, the diffusion coefficient, was significantly lower in the HCC group than in the ICC group, and was also the most effective parameter in distinguishing the two types of tumors. Both D and DDC have been reported to be diffusion coefficients, decreasing with the increased limitation of water diffusion in the tumor microstructure [50]. The other two parameters obtainable from the FROC model have been reported to be β and μ, which describe the heterogeneity in voxels and the average free range of the diffusion movement, respectively. Our results have shown no significant difference in β and μ values between the groups. These two parameters may be insufficiently sensitive to detect the differences in heterogeneity and diffusion speed between the compact cell structure and high cell proliferation of HCC and ICC [51]. However, β and μ have been reported to highlight effectively the different degrees of tumor heterogeneity to allow the differential diagnosis of various types of tumors, such as high- and low-grade urothelial bladder carcinomas, pediatric brain tumors, or benign and malignant breast tumors [52 - 54].

In this prospective clinical study, the results showed the mean DDC values from the SEM model and the D values from the FROC model to be statistically significant between the HCC and ICC groups. DDC and D values showed superior diagnostic efficiency, which initially confirmed that the SEM and FROC models could reflect different histopathological features and the complex heterogeneity of tumor tissues. Therefore, these models can provide a valuable basis for the preoperative differential diagnosis of HCC and ICC, as well as for the formulation of personalized treatment plans. They have also been found to be superior to the ADC values derived from the traditional single-index model.

This study has involved some limitations. The images obtained using free-breathing navigation during the MRI scanning could minimize motion artifacts; however, after the parameter maps of the FROC model were obtained with multiple b-values, the interference of motion artifacts could have been magnified [51]. Moreover, the ICC group was relatively small, and its size may have affected the accuracy of β and μ values. Both DDC and D could indicate the degree of cell density; however, these two parameters were not consistent in our results, possibly due to discrepancies between the fitting formula of the SEM and FROC models or the small sample size. In addition, MRI images and histopathological slides could not be accurately matched. In their study, Shan *et al*. provided comprehensive and up-to-date data on liver cancer stage at diagnosis in China, emphasizing the importance of cancer awareness and early detection programs [55]. In our study, the sample size was insufficient, with most patients with liver cancer diagnosed in the middle or late stages. We plan to expand the sample size across different stages of liver cancer and use the SEM and FROC models for early detection and analysis.

CONCLUSION

The DDC and D diffusion parameters from the SEM and FROC models, respectively, appeared to have higher diagnostic efficiencies of HCC and ICC than the traditional ADC from the mono-exponential model; these parameters may be used to improve the accuracy of the preoperative imaging diagnosis and help guide personalized treatment.

AUTHORS' CONTRIBUTION

J.X., L.L., H.J.: Study conception and design; C.L., Y.C.: Data collection; Q.C.: Analysis and interpretation of results.

LIST OF ABBREVIATIONS

HCC	=	Hepatocellular Carcinoma
ICC	=	Intrahepatic Cholangiocarcinoma
MRI	=	Magnetic Resonance Imaging
SEM	=	Stretched Exponential Model
FROC	=	Fractional Order Calculus

ETHICS APPROVAL AND CONSENT TO PARTICIPATE

This study was approved by the medical ethics committee of the First Affiliated Hospital of Guangxi Medical University (approval number: 2022-KY-E-271).

HUMAN AND ANIMAL RIGHTS

All human research procedures followed were in accordance with the ethical standards of the committee responsible for human experimentation (institutional and national), and with the Helsinki Declaration of 1975, as revised in 2013.

CONSENT FOR PUBLICATION

All patients provided written informed consent.

STANDARDS OF REPORTING

STROBE and SAGER guidelines were followed.

AVAILABILITY OF DATA AND MATERIALS

The data supporting the findings of the article were taken from the database of the First Affiliated Hospital of Guangxi Medical University, China.

FUNDING

This study was supported by the National Natural Science Foundation of China (grant number: 82060310).

CONFLICT OF INTEREST

The authors declare no conflict of interest, financial or otherwise.

ACKNOWLEDGEMENTS

The authors would like to thank Editage (www.editage.cn) for the English language editing of the paper.

REFERENCES

[1] Orcutt ST, Anaya DA. Liver resection and surgical strategies for management of primary liver cancer. Cancer Contr 2018; 25(1): 1073274817744621. [http://dx.doi.org/10.1177/1073274817744621] [PMID: 29327594]

[2] Torimura T, Iwamoto H. Treatment and the prognosis of hepatocellular carcinoma in Asia. Liver Int 2022; 42(9): 2042-54. [http://dx.doi.org/10.1111/liv.15130] [PMID: 34894051]

[3] Chang Y, Jeong SW, Young Jang J, Jae Kim Y. Recent updates of transarterial chemoembolilzation in hepatocellular carcinoma. Int J Mol Sci 2020; 21(21): 8165. [http://dx.doi.org/10.3390/ijms21218165] [PMID: 33142892]

[4] Ohama H, Hiraoka A, Tada F, *et al.* Comparison of surgical resection and percutaneous ultrasonographic guided radiofrequency ablation for initial recurrence of hepatocellular carcinoma in early stage following curative treatment. Cancers (Basel) 2022; 14(22): 5524. [http://dx.doi.org/10.3390/cancers14225524] [PMID: 36428616]

[5] Jiang C, Sun XD, Qiu W, Chen YG, Sun DW, Lv GY. Conversion therapy in liver transplantation for hepatocellular carcinoma: What's new in the era of molecular and immune therapy? Hepatobiliary Pancreat Dis Int 2023; 22(1): 7-13. [http://dx.doi.org/10.1016/j.hbpd.2022.10.006] [PMID: 36825482]

[6] Rizzo A, Ricci AD, Brandi G. Trans-arterial chemoembolization plus systemic treatments for hepatocellular carcinoma: An update. J Pers Med 2022; 12(11): 1788. [http://dx.doi.org/10.3390/jpm12111788] [PMID: 36579504]

[7] Kong D, Liu C, Miao X, Wang Y, Ding X, Gong W. Current statuses of molecular targeted and immune checkpoint therapies in hepatocellular carcinoma. Am J Cancer Res 2020; 10(5): 1522-33. [PMID: 32509395]

[8] Khaled NB, Seidensticker M, Ricke J, *et al.* Atezolizumab and bevacizumab with transarterial chemoembolization in hepatocellular

carcinoma: The DEMAND trial protocol. Future Oncol 2022; 18(12): 1423-35.
[http://dx.doi.org/10.2217/fon-2021-1261] [PMID: 35081747]

[9] El-Diwany R, Pawlik TM, Ejaz A. Intrahepatic Cholangiocarcinoma. Surg Oncol Clin N Am 2019; 28(4): 587-99.
[http://dx.doi.org/10.1016/j.soc.2019.06.002] [PMID: 31472907]

[10] Kelley RK, Bridgewater J, Gores GJ, Zhu AX. Systemic therapies for intrahepatic cholangiocarcinoma. J Hepatol 2020; 72(2): 353-63.
[http://dx.doi.org/10.1016/j.jhep.2019.10.009] [PMID: 31954497]

[11] Edeline J, Lamarca A, McNamara MG, *et al.* Locoregional therapies in patients with intrahepatic cholangiocarcinoma: A systematic review and pooled analysis. Cancer Treat Rev 2021; 99: 102258.
[http://dx.doi.org/10.1016/j.ctrv.2021.102258] [PMID: 34252720]

[12] Kim SY. Preoperative radiologic evaluation of Cholangiocarcinoma. Korean J Gastroenterol 2017; 69(3): 159-63.
[http://dx.doi.org/10.4166/kjg.2017.69.3.159] [PMID: 28329917]

[13] Tang L, Zhou XJ. Diffusion MRI of cancer: From low to high b□ values. J Magn Reson Imaging 2019; 49(1): 23-40.
[http://dx.doi.org/10.1002/jmri.26293] [PMID: 30311988]

[14] Kim PH, Yoon HM, Jung AY, Lee JS, Cho YA. Diagnostic performance of diffusion-weighted imaging for evaluation of bowel inflammation in paediatric inflammatory bowel disease: A systematic review and meta-analysis. J Crohn's Colitis 2022; 16(1): 68-78.
[http://dx.doi.org/10.1093/ecco-jcc/jjab111] [PMID: 34159379]

[15] Habre C, Botti P, Laurent M, Ceroni D, Toso S, Hanquinet S. Benefits of diffusion-weighted imaging in pediatric acute osteoarticular infections. Pediatr Radiol 2022; 52(6): 1086-94.
[http://dx.doi.org/10.1007/s00247-022-05329-3] [PMID: 35376979]

[16] Sheng H, Wang X, Jiang M, Zhang Z. Deep learning□based diffusion□weighted magnetic resonance imaging in the diagnosis of Ischemic Penumbra in early cerebral infarction. Contrast Media Mol Imaging 2022; 2022(1): 6270700.
[http://dx.doi.org/10.1155/2022/6270700] [PMID: 35291425]

[17] Ueno Y, Tamada T, Sofue K, Murakami T. Diffusion and quantification of diffusion of prostate cancer. Br J Radiol 2022; 95(1131): 20210653.
[http://dx.doi.org/10.1259/bjr.20210653] [PMID: 34538094]

[18] Yoshida S, Takahara T, Arita Y, Sakaino S, Katahira K, Fujii Y. Whole□body diffusion□weighted magnetic resonance imaging: Diagnosis and follow up of prostate cancer and beyond. Int J Urol 2021; 28(5): 502-13.
[http://dx.doi.org/10.1111/iju.14497] [PMID: 33676376]

[19] Bennett KM, Schmainda KM, Bennett RT, Rowe DB, Lu H, Hyde JS. Characterization of continuously distributed cortical water diffusion rates with a stretched-exponential model. Magn Reson Med 2003; 50(4): 727-34.
[http://dx.doi.org/10.1002/mrm.10581] [PMID: 14523958]

[20] Zhou XJ, Gao Q, Abdullah O, Magin RL. Studies of anomalous diffusion in the human brain using fractional order calculus. Magn Reson Med 2010; 63(3): 562-9.
[http://dx.doi.org/10.1002/mrm.22285] [PMID: 20187164]

[21] Jin YN, Zhang Y, Cheng JL, Zheng DD, Hu Y. Monoexponential, Biexponential, and stretched□exponential models using diffusion□weighted imaging: A quantitative differentiation of breast lesions at 3.0T. J Magn Reson Imaging 2019; 50(5): 1461-7.
[http://dx.doi.org/10.1002/jmri.26729] [PMID: 30919518]

[22] Ren H, Liu Y, Lu J, *et al.* Evaluating the clinical value of MRI multi-model diffusion-weighted imaging on liver fibrosis in chronic hepatitis B patients. Abdom Radiol (NY) 2021; 46(4): 1552-61.
[http://dx.doi.org/10.1007/s00261-020-02806-x] [PMID: 33051757]

[23] Fujimoto K, Noda Y, Kawai N, *et al.* Comparison of mono-exponential, bi-exponential, and stretched exponential diffusion-weighted MR imaging models in differentiating hepatic hemangiomas from liver metastases. Eur J Radiol 2021; 141: 109806.
[http://dx.doi.org/10.1016/j.ejrad.2021.109806] [PMID: 34120012]

[24] Kim J, Yoon H, Lee MJ, *et al.* Clinical utility of mono-exponential model diffusion weighted imaging using two b-values compared to the bi- or stretched exponential model for the diagnosis of biliary atresia in infant liver MRI. PLoS One 2019; 14(12): e0226627.
[http://dx.doi.org/10.1371/journal.pone.0226627] [PMID: 31852012]

[25] Li H, Wang L, Zhang J, Duan Q, Xu Y, Xue Y. Evaluation of microvascular invasion of hepatocellular carcinoma using whole-lesion histogram analysis with the stretched-exponential diffusion model. Br J Radiol 2022; 95(1132): 20210631.
[http://dx.doi.org/10.1259/bjr.20210631] [PMID: 34928172]

[26] Yang H, Ge X, Zheng X, *et al.* Predicting Grade of Esophageal Squamous Carcinoma: Can stretched exponential model-based dwi perform better than Bi-Exponential and Mono-Exponential model? Front Oncol 2022; 12: 904625.
[http://dx.doi.org/10.3389/fonc.2022.904625] [PMID: 35912203]

[27] Sheng R, Zhang Y, Sun W, *et al.* Staging chronic hepatitis b related liver fibrosis with a fractional order calculus diffusion model. Acad Radiol 2022; 29(7): 951-63.
[http://dx.doi.org/10.1016/j.acra.2021.07.005] [PMID: 34429260]

[28] Shao X, An L, Liu H, *et al.* Cervical carcinoma: Evaluation using diffusion MRI with a fractional order calculus model and its correlation with Histopathologic findings. Front Oncol 2022; 12: 851677.
[http://dx.doi.org/10.3389/fonc.2022.851677] [PMID: 35480091]

[29] Magin RL, Hall MG, Karaman MM, Vegh V. Fractional calculus models of magnetic resonance phenomena: Relaxation and diffusion. Crit Rev Biomed Eng 2020; 48(5): 285-326.
[http://dx.doi.org/10.1615/CritRevBiomedEng.2020033925] [PMID: 33639049]

[30] Liu G, Lu Y, Dai Y, *et al.* Comparison of mono-exponential, bi-exponential, kurtosis, and fractional-order calculus models of diffusion-weighted imaging in characterizing prostate lesions in transition zone. Abdom Radiol (NY) 2021; 46(6): 2740-50.
[http://dx.doi.org/10.1007/s00261-020-02903-x] [PMID: 33388809]

[31] Li Z, Dan G, Tammana V, *et al.* Predicting the aggressiveness of peripheral zone prostate cancer using a fractional order calculus diffusion model. Eur J Radiol 2021; 143: 109913.
[http://dx.doi.org/10.1016/j.ejrad.2021.109913] [PMID: 34464907]

[32] Xu J, Ren Y, Zhao X, *et al.* Incorporating multiple magnetic resonance diffusion models to differentiate low- and high-grade adult gliomas: A machine learning approach. Quant Imaging Med Surg 2022; 12(11): 5171-83.
[http://dx.doi.org/10.21037/qims-22-145] [PMID: 36330178]

[33] Vidić I, Egnell L, Jerome NP, *et al.* Modeling the diffusion□weighted imaging signal for breast lesions in the b = 200 to 3000 s/mm ^{2} range: Quality of fit and classification accuracy for different representations. Magn Reson Med 2020; 84(2): 1011-23.
[http://dx.doi.org/10.1002/mrm.28161] [PMID: 31975448]

[34] Xie J, Li C, Chen Y, *et al.* Potential value of the stretched exponential and fractional order calculus model in discriminating between Hepatocellular Carcinoma and Intrahepatic Cholangiocarcinoma: An animal experiment of Orthotopic Xenograft nude mice. Curr Med Imaging 2023; 20: e220323214867.
[http://dx.doi.org/10.2174/1573405619666230322123117] [PMID: 36946482]

[35] Xu R, Wu Q, Gong Y, Wu Y, Chi Q, Sun D. A novel prognostic target-gene signature and nomogram based on an integrated bioinformatics analysis in hepatocellular carcinoma. Biocell 2022; 46(5): 1261-88.
[http://dx.doi.org/10.32604/biocell.2022.018427]

[36] Peng B, Ge Y, Yin G. A novel prognostic gene signature, nomogram and immune landscape based on tanshinone IIA drug targets for hepatocellular carcinoma: Comprehensive bioinformatics analysis and *in vitro* experiments. Biocell 2023; 47(7): 1519-35.
[http://dx.doi.org/10.32604/biocell.2023.027026]

[37] Suo S, Yin Y, Geng X, *et al.* Diffusion-weighted MRI for predicting pathologic response to neoadjuvant chemotherapy in breast cancer: Evaluation with mono-, bi-, and stretched-exponential models. J Transl Med 2021; 19(1): 236.
[http://dx.doi.org/10.1186/s12967-021-02886-3] [PMID: 34078388]

[38] Kitazume Y, Tsuchiya J, Takenaka K, *et al.* High b-value computed diffusion-weighted imaging for differentiating bowel inflammation in Crohn's disease. Eur J Radiol 2020; 133: 109362.
[http://dx.doi.org/10.1016/j.ejrad.2020.109362] [PMID: 33129103]

[39] Nagaraja N. Diffusion weighted imaging in acute ischemic stroke: A review of its interpretation pitfalls and advanced diffusion imaging application. J Neurol Sci 2021; 425: 117435.
[http://dx.doi.org/10.1016/j.jns.2021.117435] [PMID: 33836457]

[40] Iima M, Le Bihan D. Clinical intravoxel incoherent motion and diffusion MR imaging: Past, present, and future. Radiology 2016; 278(1): 13-32.
[http://dx.doi.org/10.1148/radiol.2015150244] [PMID: 26690990]

[41] Zhang J, Suo S, Liu G, *et al.* Comparison of monoexponential, biexponential, stretched-exponential, and kurtosis models of diffusion-weighted imaging in differentiation of renal solid masses. Korean J Radiol 2019; 20(5): 791-800.
[http://dx.doi.org/10.3348/kjr.2018.0474] [PMID: 30993930]

[42] Çabuk F, Başsüllü N, Türkmen İ, *et al.* The prognostic relationship between histopathological and immunohistochemical features of

hepatocellular carcinoma, intrahepatic cholangiocarcinoma and mixed type. Pol J Pathol 2020; 71(2): 79-86.
[http://dx.doi.org/10.5114/pjp.2020.97015] [PMID: 32729298]

[43] Gilles H, Garbutt T, Landrum J. Hepatocellular Carcinoma. Crit Care Nurs Clin North Am 2022; 34(3): 289-301.
[http://dx.doi.org/10.1016/j.cnc.2022.04.004] [PMID: 36049848]

[44] Xue R, Chen L, Zhang C, *et al.* Genomic and transcriptomic profiling of combined Hepatocellular and Intrahepatic Cholangiocarcinoma reveals distinct molecular subtypes. Cancer Cell 2019; 35(6): 932-947.e8.
[http://dx.doi.org/10.1016/j.ccell.2019.04.007] [PMID: 31130341]

[45] Zhang J, Xing X, Wang Q, Chen Y, Yuan H, Lang N. Preliminary study of monoexponential, biexponential, and stretched-exponential models of diffusion-weighted MRI and diffusion kurtosis imaging on differential diagnosis of spinal metastases and chordoma. Eur Spine J 2022; 31(11): 3130-8.
[http://dx.doi.org/10.1007/s00586-022-07269-w] [PMID: 35648206]

[46] Bai Y, Lin Y, Tian J, *et al.* Grading of Gliomas by using Monoexponential, Biexponential, and stretched exponential diffusion-weighted MR imaging and diffusion Kurtosis MR imaging. Radiology 2016; 278(2): 496-504.
[http://dx.doi.org/10.1148/radiol.2015142173] [PMID: 26230975]

[47] Witjes CDM, Willemssen FEJA, Verheij J, *et al.* Histological differentiation grade and microvascular invasion of hepatocellular carcinoma predicted by dynamic contrast□enhanced MRI. J Magn Reson Imaging 2012; 36(3): 641-7.
[http://dx.doi.org/10.1002/jmri.23681] [PMID: 22532493]

[48] Shi B, Xue K, Yin Y, *et al.* Grading of clear cell renal cell carcinoma using diffusion MRI with a fractional order calculus model. Acta Radiol 2023; 64(1): 421-30.
[http://dx.doi.org/10.1177/02841851211072482] [PMID: 35040361]

[49] Karaman MM, Tang L, Li Z, Sun Y, Li JZ, Zhou XJ. *In vivo* assessment of Lauren classification for gastric adenocarcinoma using diffusion MRI with a fractional order calculus model. Eur Radiol 2021; 31(8): 5659-68.
[http://dx.doi.org/10.1007/s00330-021-07694-3]

[50] Guo Y, Chen J, Zhang Y, *et al.* Differentiating Cytokeratin 19 expression of hepatocellular carcinoma by using multi-b-value diffusion-weighted MR imaging with mono-exponential, stretched exponential, intravoxel incoherent motion, diffusion kurtosis imaging and fractional order calculus models. Eur J Radiol 2022; 150: 110237.
[http://dx.doi.org/10.1016/j.ejrad.2022.110237] [PMID: 35278979]

[51] Zhang A, Hu Q, Song J, Dai Y, Wu D, Chen T. Value of non-Gaussian diffusion imaging with a fractional order calculus model combined with conventional MRI for differentiating histological types of cervical cancer. Magn Reson Imaging 2022; 93: 181-8.
[http://dx.doi.org/10.1016/j.mri.2022.08.014] [PMID: 35988835]

[52] Sui Y, Wang H, Liu G, *et al.* Differentiation of low- and high-grade pediatric brain tumors with high b-value diffusion-weighted MR imaging and a fractional order calculus model. Radiology 2015; 277(2): 489-96.
[http://dx.doi.org/10.1148/radiol.2015142156] [PMID: 26035586]

[53] Wang C, Wang G, Zhang Y, *et al.* Differentiation of benign and malignant breast lesions using diffusion-weighted imaging with a fractional-order calculus model. Eur J Radiol 2023; 159: 110646.
[http://dx.doi.org/10.1016/j.ejrad.2022.110646] [PMID: 36577184]

[54] Feng C, Wang Y, Dan G, *et al.* Evaluation of a fractional-order calculus diffusion model and bi-parametric VI-RADS for staging and grading bladder urothelial carcinoma. Eur Radiol 2022; 32(2): 890-900.
[http://dx.doi.org/10.1007/s00330-021-08203-2] [PMID: 34342693]

[55] Shan T, Ran X, Li H, *et al.* Disparities in stage at diagnosis for liver cancer in China. J Natl Cancer Cent 2023; 3(1): 7-13.
[http://dx.doi.org/10.1016/j.jncc.2022.12.002] [PMID: 39036312]